

Vortices in Dense Self-Assembled Hole Arrays

G. W. Crabtree, U. Welp, Z. L. Xiao, J. S. Jiang, V. K. Vlasko-Vlasov, S. D. Bader
Materials Science Division, Argonne National Laboratory, Argonne, IL 60439

J. Liang, H. Chik, J. M. Xu
Division of Engineering and Department of Physics, Brown University, Providence, RI 02912

Abstract

We present a study of the upper critical field and pinning strength from the resistivity and magnetization of a Nb film containing a dense array of 45 nm diameter holes on a hexagonal lattice with a spacing of 101 nm. The holes were formed by self-assembly in anodic aluminum oxide (AAO) using an electrochemical procedure. Confinement effects and Little-Parks oscillations are seen above 6 K, and strong pinning with matching field effects is seen below 6 K. Above the first matching field interstitial vortices coexist with vortices trapped in the hole array. Pinning in the Nb films with hole arrays is enhanced by two orders of magnitude over that in continuous Nb films. At low temperature, flux avalanches are observed and imaged using the magneto-optical Faraday effect.

Introduction

Vortices in superconductors have received much attention in recent years for their macroscopic collective behavior [1-4]. Each vortex is a well defined structural unit containing one quantum of flux that interacts with its neighbors through long range electrodynamic forces. Abrikosov [5] showed in the 1950s that these repulsive interactions lead to a regular hexagonal lattice in the absence of other interactions. At finite temperature, thermal energy competes with the vortex interaction energy and can melt the Abrikosov lattice to a liquid of lines. Defects in the superconductor introduce random pinning into the vortex system, disordering the lattice to glassy states. These collective lattice, liquid, and glassy states provide a rich phase diagram of first and second order transitions that is analogous in many ways to that of ordinary atomic matter. Vortex matter at macroscopic scales provides new insight into the collective behavior of interacting systems subject to thermal and quenched disorder.

Vortex matter at mesoscopic scales offers equally interesting insights into the behavior of confined systems. Confinement occurs in superconducting samples whose size or internal structure is on the order of the Abrikosov lattice constant, $L \sim (\Phi_0/H)^{1/2}$. In this case the superconductor provides an additional force due to its surface or its internal structure that strongly influences the behavior of individual vortices. Two cases have been explored to date. The first is a small sample that can accept only a few vortices, a *superconducting dot* [6,7].

Vortices in such dots dramatically alter their behavior, entering discretely in single units, forming shell structures instead of the hexagonal lattice in macroscopic samples, and transforming from multivortex configurations to giant vortex configurations containing several quanta of undifferentiated flux. These superconducting dots offer many new directions for studying single vortex behavior, with strong analogies to single electron behavior in quantum dots.

The second approach to exploring single vortex behavior superimposes a template on the superconductor, typically a periodic array of pinning centers that strongly attracts the vortices. This template may consist of magnetic dots, patterned radiation damage, or holes, often referred to as *antidots*. The template of holes guides the formation of the vortex configuration much as epitaxial growth guides the placement of atoms on a substrate. Although the size of a template may be large, its structure of holes strongly influences each of the individual vortices it supports. Hole arrays produce a rich variety of commensurate and incommensurate behavior in the vortex system [8-16].

In this paper we describe studies of vortex behavior in dense hole arrays prepared by self assembly. The hole density in these arrays is up to a factor of 100 higher than in typical lithographically prepared arrays. The high density of holes puts the templated vortex array into the strongly interacting limit, where vortex-vortex interactions reinforce the natural pinning of the template. We find several effects not seen in larger micron-sized hole arrays produced by lithography, including dimensional crossover from 1D to 2D superconductivity, Little-Parks oscillations of the upper critical field, and strong pinning of the templated vortex array at low temperature.

Fabrication

Our hole arrays were prepared by self assembly of pores in anodic aluminum oxide (AAO). The anodization of high purity Al films was carried out in a two step process. [17] After anodization, the pores formed a regular hexagonal array in the aluminum oxide membrane. The membrane was covered with a 100 nm film of Nb deposited by magnetron sputtering, followed by a 10 nm thick Ag capping layer. Figure 1 shows an SEM image of the cleaved AAO membrane with the Nb and Ag deposited layers, taken at 45° to reveal the hole pattern in the membrane and the overlayers on the surface. The holes in the membrane are of uniform diameter and spacing, forming a hexagonal pattern that maintains its hexatic orientation over microns before meeting a grain with different orientation. A boundary between grains is marked in the image. The Nb and Ag layers deposit on the walls between the pores, leaving holes of 45 nm diameter and 101 nm spacing. The Nb deposits in a columnar manner, as indicated by the clumping structures at the intersection of walls and the lines between clumps visible in the image. For reference, continuous Nb films of the same thickness were deposited on sapphire substrates.

Superconducting Transition and Upper Critical Field

The superconducting transition in fields up to 7.5 kG was studied resistively in field cooling, as shown in Figure 2. The resistive transition in zero field is about 200 mK wide and is centered at 6.82 K. For comparison, the transition of the continuous reference film is at 7.5 K. The lower transition for the patterned film could be due to proximity with the normal Ag cap layer, and to

contamination arising from the AAO interface. The resistive transition in field maintains its shape, giving an accurate measure of H_{c2} taken as the midpoint of the transition. The fields marked H_n indicate the matching fields, where the vortex density is n times the hole density. The clustering of the resistive curves about these fields reflects the Little-Parks oscillations described in more detail below.

The upper critical field derived from these data is plotted in Figure 3, along with that of the continuous reference film. Apart from a reduction in T_c , the AAO film shows two interesting features near T_c : a downward curvature and a set of three oscillations. The downward curvature is reminiscent of dimensional crossover in confined samples. Superconducting confinement occurs when the growth of the coherence length with increasing temperature is cut off by the finite sample dimension. Then the conventional temperature dependence of the upper critical field, $H_{c2} = \Phi_0/2\pi\xi^2(T)$ is replaced by $H_{c2} = \Phi_0/2\pi w\xi(T)$, where w is the confining sample dimension. As $\xi(T) = \xi(0)/(T/T_c - 1)^{1/2}$, the conventional linear temperature dependence is replaced by a parabolic one in confined samples. In our samples, the limiting length is the width of the walls between the holes, approximately 55 nm as measured from SEM images. Fitting the data of Figure 3 to the thin film formula [18]

$$H_{c2} = \sqrt{12} \Phi_0 / 2\pi w \xi(T)$$

yields $\xi(0) \sim 10$ nm (dashed line). Below approximately 6 K, H_{c2} becomes linear, indicating that confinement is no longer active, ie $\xi(T) < w$. The Ginzburg-Landau temperature dependence of $\xi(T)$ is consistent with this condition for $\xi(0) \sim 10$ nm. Extrapolation of the linear part of the curve to $T=0$ and using the conventional formula $H_{c2} = \Phi_0/2\pi\xi^2(T)$ yields the same value $\xi(0) \sim 10$ nm. The mean free path l can be obtained from the dirty limit expression $l = 1.38 \xi(0)/\xi_0$ where ξ_0 is the BCS coherence length, 38 nm [19]. The Ginzburg-Landau parameter κ can be estimated from $\kappa = 0.72 \lambda_L/l \sim 7$ where $\lambda_L = 39$ nm is the London penetration depth [19]. These values of the characteristic lengths imply that $\lambda(0)/a \sim 0.7$, indicating that vortices trapped in neighboring holes interact strongly, and that $\xi(0)/r = 0.4$ where r is the radius of the hole.

Oscillations in the upper critical field are seen in Figure 3 for $T > 6$ K. These oscillations reflect the clustering of the resistive transitions around the fields H_n for $n = 1, 2$ and 3 in Figure 2. These fields correspond to the matching fields of the hole array, where each primitive cell of the array contains 1, 2 or 3 flux quanta. The lowest matching field H_1 can be estimated from the lattice constant of the hexagonal hole array, $H_1 = 2\Phi_0/a^2\sqrt{3} = 2255$ Oe, in good agreement with the observed oscillation period. The oscillations occur in the 1D region above 6 K. In this region, the condition $\xi(T) > w$ prevents the formation of vortices in the superconducting walls between the holes. Here the superconductor acts as a wire network, transporting current but not supporting vortices. The periodic oscillations in H_{c2} are Little-Parks oscillations [20] arising from the supercurrent flow in the network [21-25] required to maintain an integer number of flux quanta in each unit cell of the hole array. These supercurrents carry kinetic energy that decreases the condensation energy and therefore lowers the transition temperature. At the matching fields, there is integer flux in each hole, the supercurrents vanish, and the transition temperature is a maximum.

The oscillations in H_{c2} are more clearly seen in Figure 4, where the parabolic background has been subtracted. There the maxima in T_c are clearly seen to occur at the matching fields, as expected for Little Parks oscillations. The T_c variation can be fit quantitatively to the phenomenological model derived from the Ginzburg Landau equations [25],

$$\Delta T_c/T_c = -(\xi(0)/a)^2 [1/4 - (\Phi/\Phi_0 - n - 1/2)^2]$$

where Φ is the flux per unit cell, a is the lattice constant of the hole array, and $n = 1, 2, 3, \dots$ is the number of flux quanta per cell. This fit is shown as the dotted lines in Figure 4. The fit value of $\xi(0) = 15$ nm is in reasonable agreement with the values derived from the H_{c2} temperature dependence in the confined 1D region above 6 K and the 2D region below 6 K.

In the lowest parabola below the first matching field, the data deviate significantly from the fit. These deviations could indicate the presence of ordered states at partial filling where 1/3 and 2/3 of the holes are filled with flux. Such ordered states at half filling have been seen in square arrays with micron size spacing using scanning Hall probe microscopy and Lorentz imaging. [26,27,28] Ordered states at partial filling offer many possibilities for studying the energetics of antiphase domain formation and the geometry of the boundaries between them.

Pinning and Critical Currents

The pinning behavior of dense Nb-AAO differs markedly from that of micron-sized hole arrays. Figure 5 shows magnetization curves for the field perpendicular to the AAO array taken on sweeping the field up and down after zero field cooling. The first matching field is clearly seen at 6.5 K, the second at 5.5 K, and the third at 4.5 K. The matching field effects appear as steps in the magnetization that become higher at lower temperature, in contrast to the behavior of micron-sized hole arrays where matching effects disappear just a few tenths of a K below T_c . In the Nb-AAO arrays the pinning force of the holes is substantial and increases as the temperature is lowered, as seen by the increased hysteresis. Because the AAO hole array is approximately 100 times denser than lithographically prepared templates, the matching field effects and strong pinning extend to much higher fields, ~ 7.5 kG for the third matching field. In micron sized hole arrays, the matching field effects decay above a few hundred Oe. Compared to the continuous Nb film, the critical current in the Nb-AAO array is enhanced by approximately two orders of magnitude at the second matching field [16].

The origin of the strong matching effects and the high critical currents can be found in the vortex configuration in the hole array. The magnetization curves in Figure 5 allow either of two possible configurations. Beyond the first matching field, additional vortices may multiply occupy the holes [29], leaving the superconductor vortex-free, or they may enter the superconductor, leaving each hole singly occupied. Insight into the actual configuration is provided by estimates of the occupancy limit of holes of a given size in isolation and in arrays. An isolated hole can accept up to $n_s = d/4\xi(T)$ vortices, where d is the diameter of the hole and ξ is the coherence length [30]. Our estimates of d and ξ imply that $n_s = 1$ for our samples. Including the interaction energy of vortices in neighboring holes, it can be shown that [29] a triangular array of holes will accept two vortices/hole if $d^3 > 8 \xi a^2$. This condition is not satisfied for our samples, implying again that only one vortex may occupy a hole. Beyond the

first matching field, therefore, interstitial vortices appear and coexist with vortices trapped in the holes.

The configuration of the coexisting interstitial and hole-trapped vortices is determined by vortex interaction effects. The condition $\lambda(0)/a \sim 1$ implies that vortex-vortex interactions are strong at in our high density hole arrays. Thus the interstitial vortices feel a significant cage potential [31] created by the hole-trapped vortices. The minima of the cage potential are located at the centers of the equilateral triangles formed by the holes, as shown in Figure 6. There are two such sites per primitive cell of the hole array, indicated by the dotted lines. One of these sites will be occupied at the second matching field, producing a symmetric array of three interstitial vortices spaced 120° apart about each hole. At the third matching field the second interstitial site is occupied, completing the hexagonal pattern commensurate with the hole array. At higher matching fields, the energy minima of the possible interstitial configurations fit less naturally with the hexagonal hole pattern, and they are much less stable.

At 4.5 K for fields below the first matching field, the magnetization data in Figure 5 fluctuates strongly. These fluctuations are due to flux jumps or avalanches [32-35] in the vortex configuration. Such flux jumps appear where the pinning strength and magnetic field gradients are high. They arise from runaway thermal events, where the heat generated during flux motion raises the local temperature and lowers the local critical current, driving additional flux into motion. Evidence for these avalanche events can be found in the flux patterns they produce. Figure 6 shows a magneto-optical image of flux in our Nb-AAO film, taken at 4.5 K in a field of 200 Oe, in the region of the fluctuations. The penetration pattern is highly inhomogeneous in character, showing the paths of local heating and flux motion. The flux paths are intricately curved, unlike similar paths in square hole arrays with micron spacing which are rectilinear with only 90° angles [36]. The curved paths visible in Figure 6 reflect the much closer spacing of holes, enabling easy flux jumps between neighboring holes, and the hexagonal pattern of holes, where the hole density along many non-symmetry directions is high enough to support flux motion.

Discussion and Summary

The high density hole arrays presented here show several new effects not seen in micron-size hole arrays prepared by lithography. At high temperature the arrays show confinement effects arising from the narrow width w of the superconducting walls between the holes. For $\xi(T) > w$, vortices may not form in the walls and the system behaves as a wire network, showing a confined parabolic upper critical field with Little-Parks oscillations at the matching fields. At lower temperature where $\xi(T) < w$ vortices may enter the walls and the magnetization shows strong matching field effects up to $3H_1$. The hole size in our arrays accommodates only one vortex, so that interstitial vortices coexist with hole-trapped vortices above the first matching field. The condition $\lambda(0)/a \sim 1$ ensures that the interstitial vortices interact strongly with the hole-trapped vortices. The cage potential of the hole-trapped vortices creates strong pinning sites for the interstitial vortices at the centers of the triangles formed by the holes. There are two such sites per hole, accounting for the matching effects at the second and third matching field.

Pinning in these dense hole arrays is very strong, in contrast to the weak pinning of hole arrays with micron spacing. In dense arrays strong matching field effects are seen at all temperatures, showing that pinning by holes and the cage potential of vortices trapped in them dominates the random pinning of defects in the bulk Nb. Because the hole arrays are dense, the matching field is high, ~ 2.25 kG. Strong pinning persists up to the third matching field, ~ 7 kG, and down to low temperatures. This is in contrast to pinning in micron size hole arrays prepared by lithography, where pinning is only significant within a few tenths of a K of T_c and matching field effects extend only a few hundred Oe at most. The enhancement of the critical current by the Nb-AAO array is typically two orders of magnitude at the second matching field.

Dense hole arrays provide several interesting new directions. The strong pinning of dense hole arrays can be used for applications, enabling even low pinning superconductors to carry a high critical current. Operation at fields of order 1 T over a wide temperature range significantly outperforms conventional micron-size hole arrays. In high temperature superconductors like YBCO, dense hole arrays enable effective pinning of the vortex liquid, which requires pinning of every vortex in order to prevent shear motion. Using the vortex liquid for applications opens up the high temperature region above the irreversibility line of the phase diagram. In high temperature superconductors the short coherence length increases the maximum vortex occupancy of the holes, extending matching effects beyond the third matching field and creating interesting coexistence states of interstitial and hole-trapped vortices. Below the first matching field, partial filling of the holes is expected to create interesting sub-matching effects, as have been seen in micron size square hole arrays. The strong interaction of vortices in partially occupied dense arrays should lead to interesting antiphase domains and domain boundaries.

This work was supported by the U.S. Department of Energy, BES, Materials Science under contract W-31-109-ENG-38 at Argonne National Laboratory, and by the National Science Foundation under contract NSF ECS 0070019 and by the Office of Naval Research under contract N00014 001 0260 at Brown University. The SEM work was performed at the Electron Microscopy Center at ANL.

References

1. F. Bouquet, C. Marcenat, E. Steep, R. Calemczuk, W. K. Kwok, U. Welp, G. W. Crabtree, R. A. Fisher, N. E. Phillips, and A. Schilling, *Nature* **411**, 448 (2001)
2. N. Avraham, B. Khaykovich, Y. Myasoedov, M. Rappaport, H. Shtrikman, D. E. Feldman, T. Tamegai, P. H. Kes, M. Li, M. Konczykowski, K. van der Beek, and E. Zeldov, *Nature* **411**, 451 (2001)
3. W. K. Kwok, R. J. Olsson, G. Karapetrov, L. M. Paulius, W. G. Moulton, D. J. Hofman, and G. W. Crabtree, *Phys. Rev. Lett.* **84**, 3706 (2000).
4. George W. Crabtree and David R. Nelson, *Physics Today* **50** (4), 38-45 (1997).

5. Abrikosov, A. A., (1957) On the magnetic properties of superconductors of the second group, *Zh. Eksp. Teor. Fiz.* **32**, 1442-1452 [(1957) *Sov. Phys. JETP* **5**, 1174-1182].
6. A. K. Geim, S. V. Dubonos, J. J. Palacios, I. V. Grigorieva, M. Henini, and J. J. Schermer *Phys. Rev. Lett.* **85**, 1528 (2000)
7. A. K. Geim, I. V. Grigorieva, S. V. Dubonos, J. G. S. Lok, J. C. Maan, A. E. Filippov, F. M. Peeters, *Nature* **390**, 259 - 262 (1997)
8. A. T. Fiory, A. F. Hebard, and S. Somekh, *Appl. Phys. Lett.* **32**, 73 (1978).
9. M. Baert, V. V. Metlushko, R. Jonckheere, V. V. Moshchalkov, and Y. Bruynseraede, *Phys. Rev. Lett.* **74**, 3269 (1995).
10. V. V. Moshchalkov, M. Baert, V. V. Metlushko, E. Rosseel, M. J. Van Bael, K. Temst, Y. Bruynseraede, and R. Jonckheere, *Phys. Rev. B* **57**, 3615 (1998).
11. V. Metlushko, U. Welp, G. W. Crabtree, R. Osgood, and S. D. Bader, L. E. DeLong, Zhao Zhang and S. R. J. Brueck, B. Ilic, K. Chung, and P. J. Hesketh, *Phys. Rev. B* **60**, 12585 (1999).
12. José I. Martín, M. Vélez, A. Hoffmann, Ivan K. Schuller, and J. L. Vicent, *Phys. Rev. Lett.* **83**, 1022 (1999).
13. J. I. Martín, M. Vélez, J. Nogués, and Ivan K. Schuller *Phys. Rev. Lett.* **79**, 1929 (1997).
14. David J. Morgan and J. B. Ketterson *Phys. Rev. Lett.* **80**, 3614 (1998).
15. A. Hoffmann, P. Prieto, and Ivan K. Schuller, *Phys. Rev. B* **61**, 6958 (2000).
16. U. Welp, Z. L. Xiao, J. S. Jiang, V. K. Vlasko-Vlasov, S. D. Bader, G. W. Crabtree, J. Liang, H. Chik, J. M. Xu, *Phys Rev B*, In Press.
17. A. J. Yin, J. Li, W. Jian, A. J. Bennett, and J. M. Xu, *Appl. Phys. Lett.* **79**, 1039 (2001); J. Liang, H. Chik, A. Yin, and J. Xu, *J. Appl. Phys.* **91**, 2544 (2002); H. Masuda, H. Fukuda, *Science* **268**, 1466 (1995).
18. M. Tinkham, "Introduction to Superconductivity" (McGraw-Hill, New York, (1996), eq 4.51.
19. B. W. Maxfield, W. L. McLean, *Phys. Rev.* **139**, A1515 (1965).
20. R. D. Parks, W. A. Little, *Phys. Rev. A* **133**, 97 (1964).
21. M. Tinkham, David W. Abraham, and C. J. Lobb, *Phys. Rev. B* **28**, 6578 (1983).

22. Carlos W. Wilks, Rick Bojko, and Paul M. Chaikin, *Phys. Rev. B* **43**, 2721 (1991).
23. H. S. J. van der Zant, M. N. Webster, J. Romijn, and J. E. Mooij, *Phys. Rev. B* **50**, 340 (1994).
24. W. J. Elion, H. S. J. Van der Zant, J. E. Mooij, “Macroscopic Quantum Phenomena and Coherence in Superconducting Networks” (World Scientific, Singapore, 1995).
25. A. Bezryadin, B. Pannetier, *J. Low Temp. Phys.* **98**, 251 (1995).
26. S. B. Field, S. S. James, J. Barentine, V. Metlushko, G. Crabtree, H. Shtrikman, B. Ilic, and S. R. J. Brueck, *Phys. Rev. Lett.* **88**, 067003 (2002)
27. A. N. Grigorenko, G. D. Howells, and S. J. Bending, J. Bekaert, M. J. Van Bael, L. Van Look, V. V. Moshchalkov, and Y. Bruynseraede, G. Borghs, I. I. Kaya, R. A. Stradling *Phys. Rev. B* **63**, 052504 (2001).
28. K. Harada, O. Kamimura, H. Kasai, T. Matsuda, A. Tonomura, V. V. Moshchalkov, *Science* **274**, 1167 (1996).
29. A. I. Buzdin, *Phys. Rev. B* **47**, 11416 (1993).
30. G. S. Mkrtchyan, V. V. Shmidt, *Soviet Phys. JETP* **34**, 195 (1972).
31. I. B. Khal'fin, B. Ya. Shapiro, *Physica C* **207**, 359 (1993).
32. P. S. Schwartz, C. P. Bean, *J. Appl. Phys.* **39**, 4991 (1968).
33. R. G. Mints, A. L. Rakhmanov, *Rev. Mod. Phys.* **53**, 551 (1981).
34. E. R. Nowak, O. W. Taylor, Li Liu, H. M. Jaeger, and T. I. Selinder *Phys. Rev. B* **55**, 11702 (1997), *Phys. Rev. B* **55**, 11702 (1997).
35. P. Esquinazi, A. Setzer, D. Fuchs, Y. Kopelevich, E. Zeldov, and C. Assmann *Phys. Rev. B* **60**, 12454 (1999)
36. V. K. Vlasko-Vlasov, unpublished.

Figure Captions

Figure 1. SEM image of a cleaved AAO membrane covered with 100 nm overlayer of Nb and 10 nm cap layer of Ag. The holes in Nb layer are 45 nm in diameter and form a hexagonal pattern with 101 nm spacing. The line shows a grain boundary between hexagonal hole patterns of different orientation.

Figure 2. Resistive transitions of the patterned Nb film in fields from 0 to 7.5 kG, in 0.25 kG increments. Data were taken at 0.1 mA in field cooling. Note the obvious clustering of the transition curves at the fields marked H_1 , H_2 , and H_3 , which indicate Little-Parks oscillations with a period of the matching field. The upper critical field was determined from these data as the midpoint of the transition.

Figure 3. The upper critical field of the Nb-AAO hole array (triangles) and of the continuous Nb film (squares). The downward curvature above about 6 K is due to dimensional crossover from 2D behavior at low T to 1D behavior at high T. The dashed curve is a parabolic fit to the 1D behavior using the thin film formula for H_{c2} (see text).

Figure 4 Little-Parks oscillations in the upper critical field, enhanced by subtraction of the parabolic background from the data of Figure 3. The maxima in T_c occur at the matching fields H_1 , H_2 and H_3 , as expected for a wire network. The dashed line is a fit to the phenomenological network formula (see text).

Figure 5 Magnetic moment of the Nb-AAO array for the applied field perpendicular to the membrane. Data were taken in zero field cooling at the temperatures shown, with the field swept up and down. H_1 , H_2 and H_3 are the matching fields. The fluctuations at the lowest temperature are due to flux avalanches.

Figure 6 The hexagonal hole array with the positions of the minima in the cage potential of vortices trapped in the holes.

Figure 7 Magneto-optical image of flux avalanches in the Nb-AAO film, taken at 4.5 K in a field of 200 Oe.

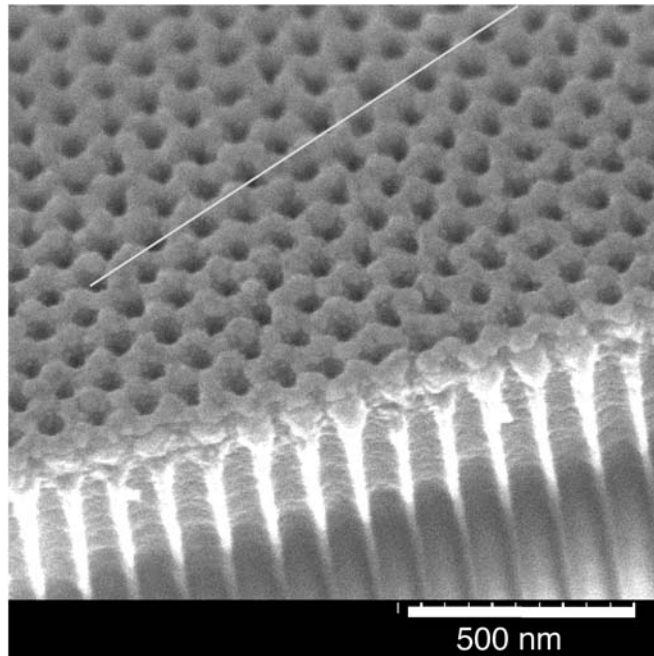


Figure 1

Crabtree et al L-24

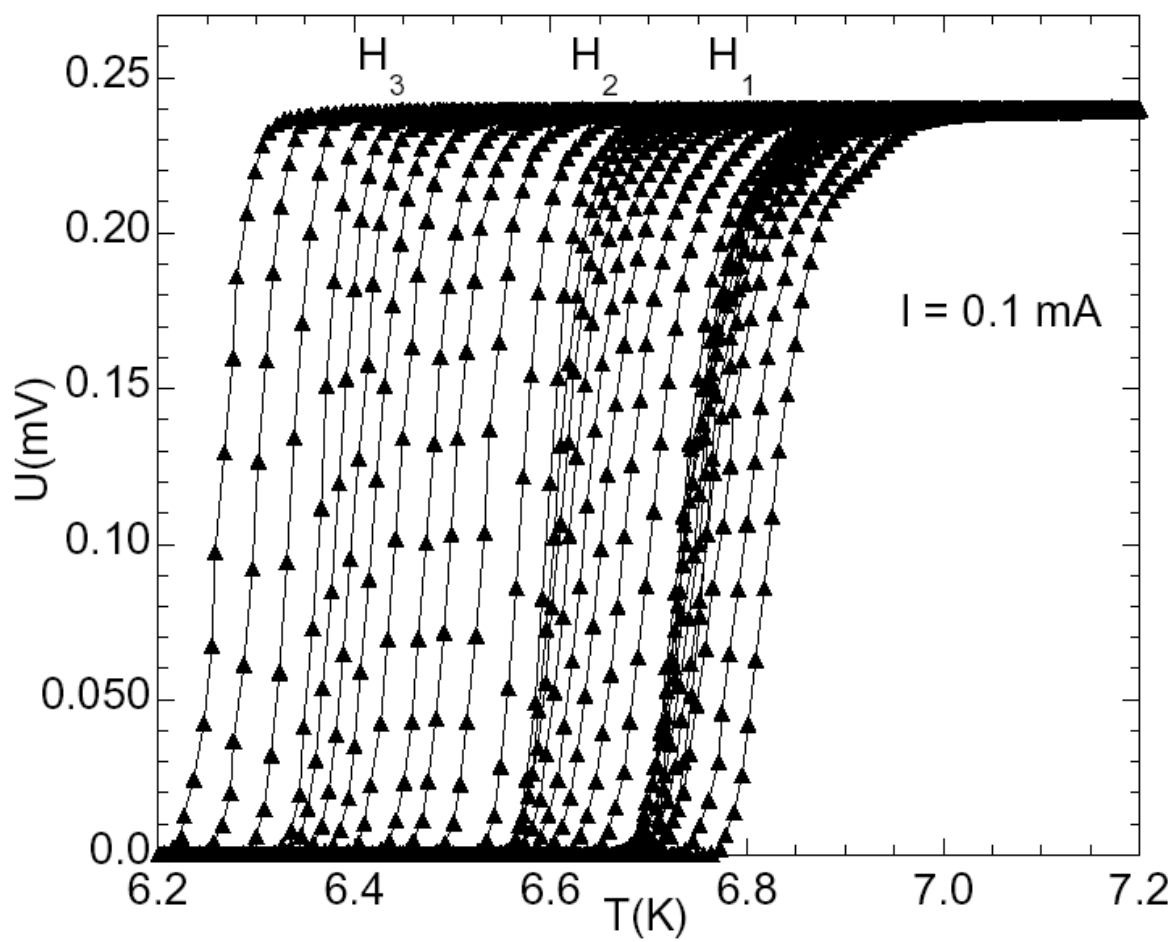


Figure 2

Crabtree et al L-24

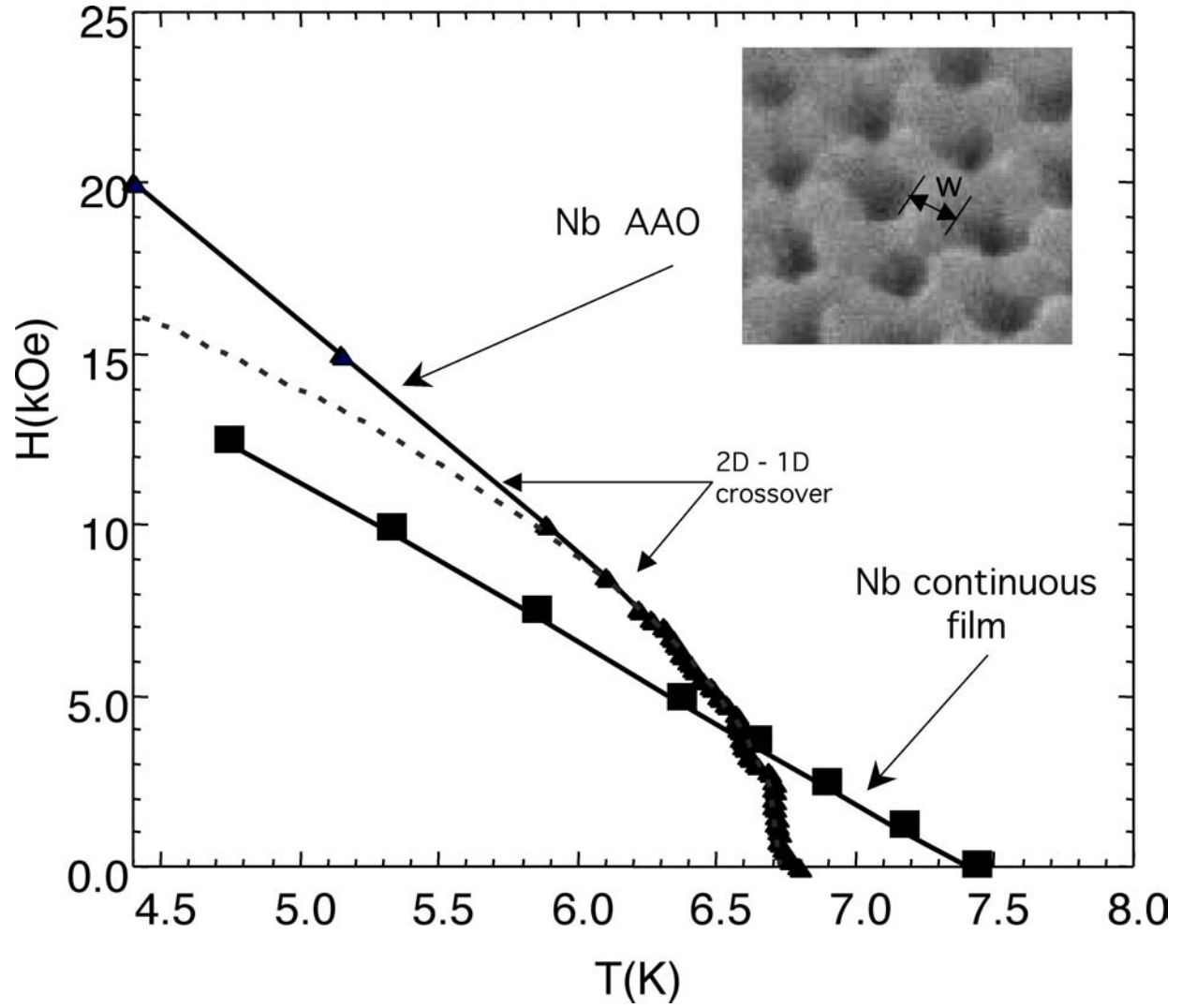


Figure 3

Crabtree et al L-24

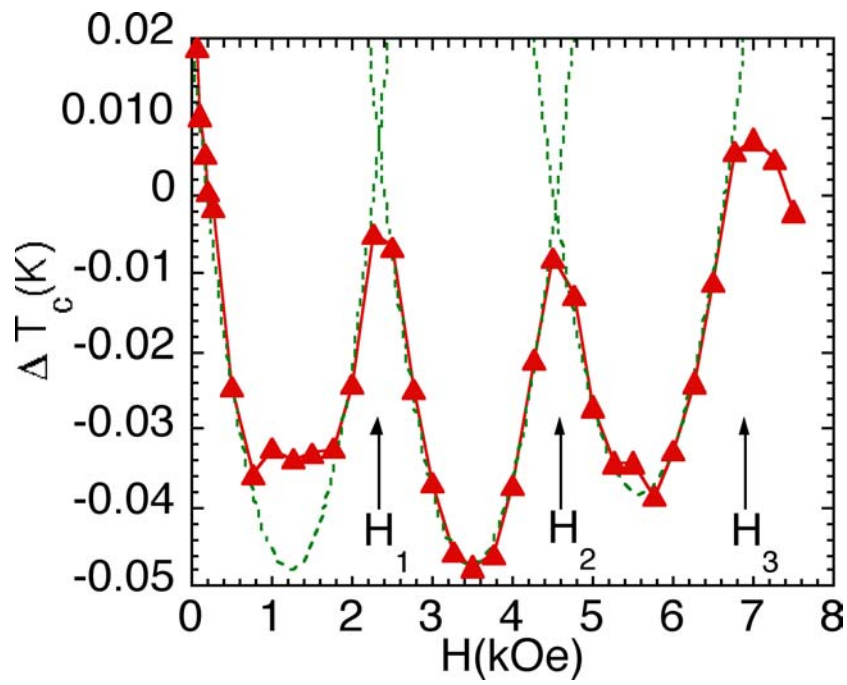


Figure 4

Crabtree et al L-24

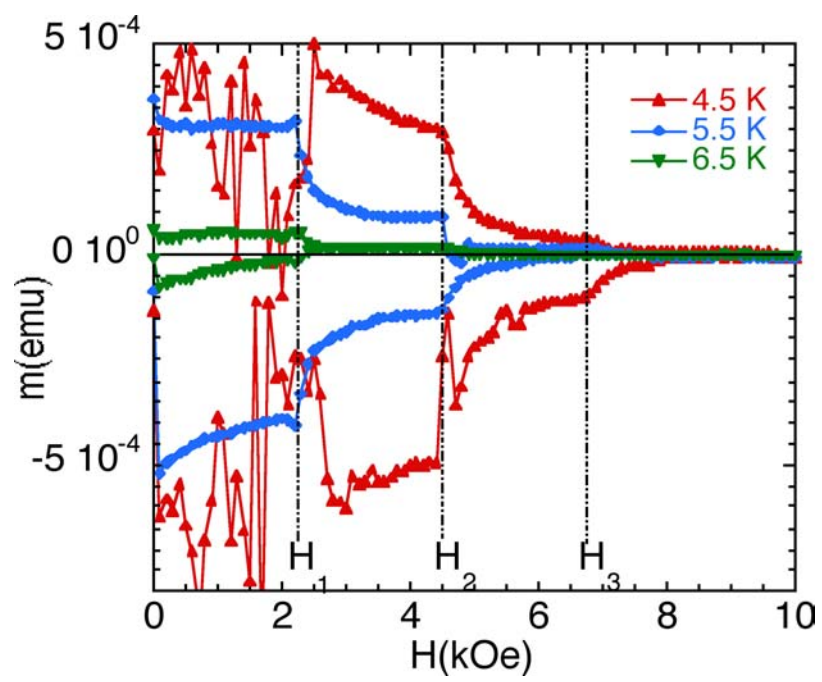


Figure 5

Crabtree et al L-24

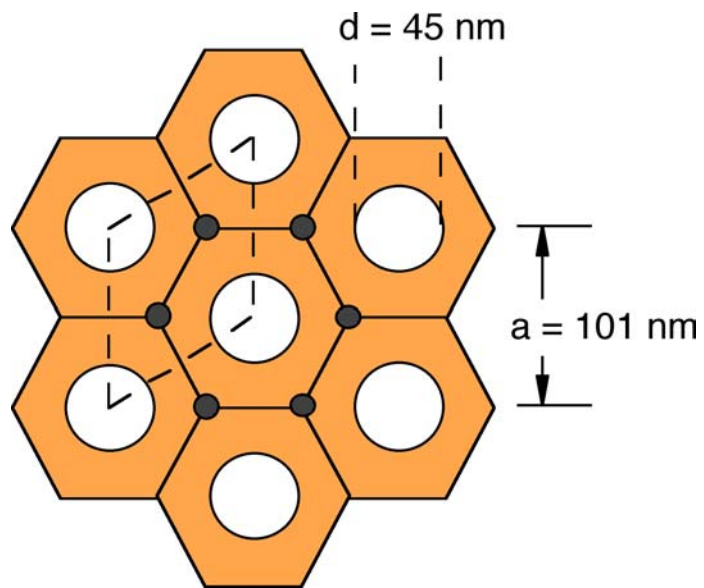
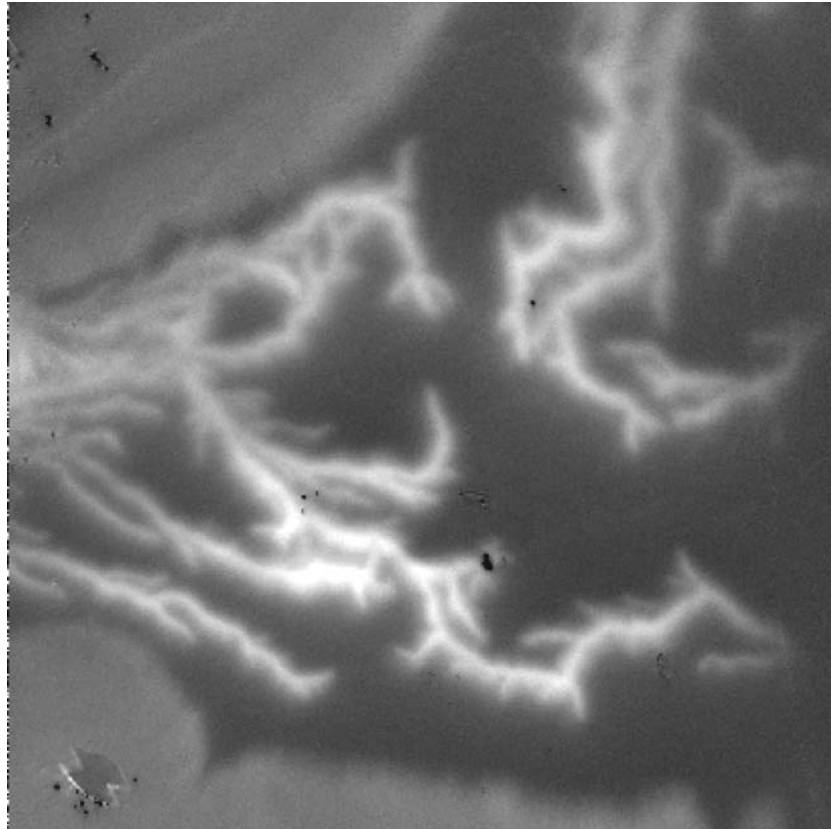


Figure 6

Crabtree et al L-24



← 450 μ →

Figure 7

Crabtree et al L-24